Al/SiC thermal spray coatings for corrosion protection of Mg–Al alloys in humid and saline environments

R. Arrabal [a,*], A. Pardo [a], M.C. Merino [a], M. Mohedano [a], P. Casajús [a], S. Merino [b]

[a] Departamento de Ciencia de Materiales, Facultad de Ciencias Químicas, Universidad Complutense, 28040, Madrid, Spain
[b] Departamento de Tecnología Industrial, Universidad Alfonso X El Sabio, 28691, Villanueva de la Cañada, Madrid, Spain

ARTICLE INFO

ABSTRACT

The corrosion behaviour of thermal spray Al/SiC coatings deposited on AZ31, AZ80 and AZ91D Mg–Al–Zn alloys was evaluated in neutral salt fog (ASTM B 117) and high relative humidity (98% RH, 50 °C) environments. The findings revealed porous as-sprayed coatings with paths providing access of the corrosive media to the magnesium substrates. This resulted in galvanic corrosion at the substrate/coating interfaces and formation of magnesium corrosion products, which eventually led to coating spalling in the case of salt fog tests after protracted times of exposure. The application of a cold-pressing post-treatment improved the corrosion performance of the coatings. Thus, in high humidity atmosphere, corrosion signs were only visible at the Al/SiC interfaces in the outermost surface of the coatings and, in salt fog environment, the galvanic corrosion of the substrates was delayed.

© 2010 Elsevier B.V. All rights reserved.

1. Introduction

Mg–Al–Zn alloys are the most commonly used magnesium alloys for transport applications [1]. Compared with aluminium or steels, these alloys present lower density, higher specific strength and, under mild conditions, they may exhibit similar or even higher corrosion resistance [2,3].

The main obstacles for increased magnesium usage are wear and corrosion resistance, but metallic and ceramic coatings can be engineered to tailor these properties [4]. The surface technologies used in order to extend the lifetime of magnesium components were recently reviewed by Gray and Luan [5]. Due to the very wide selection of coatings that can be sprayed, thermal spray technology is gaining interest as a protective method for magnesium alloys [6–8]. For instance, fabrication of aluminium thermal spray coatings on magnesium substrates is a simple, economical and pollution free method to improve the corrosion performance of magnesium alloys without altering its recyclability [9–12]. In most cases, however, thermal spraying can lead to coatings with characteristic defects such as pores, cracks or irregularities in phase distribution [13]. Therefore, mechanical, chemical and/or physical post-treatments are commonly applied in order to improve the effectiveness of the coating against

corrosion [10–12,14–17]. For example, Zhongshan [10] found that an aluminium arc spray coating with a heat post-treatment reduced the corrosion current density of the AZ31 alloy immersed in 3.5% NaCl at pH 10.5 from 2.4×10^{-1} mA cm^{-2} to 7.1×10^{-3} mA cm^{-2}. And Chiu [11] improved the corrosion resistance of the AZ31 alloy by applying a similar aluminium coating that was hot pressed and anodized.

For applications where the wear response of magnesium alloys is important, ceramic coatings are mostly used. Another alternative is to provide corrosion and wear protection by using composite coatings [18,19]. There are several examples of Al/SiC coatings deposited on magnesium substrates by various spraying technologies [13,15,20,21]. From the mechanical point of view, these coatings usually show higher hardness and wear resistance than unreinforced Al coatings or uncoated magnesium substrates. However, the presence of SiC reinforcement can decrease the corrosion resistance of the coating and facilitate the formation of brittle aluminium carbides during heat treatments [13].

In the present study, Al coatings containing 5, 15 and 30 vol.% SiC particles were deposited on Mg–Al–Zn alloys by a flame spray process and their corrosion behaviour in as-sprayed and cold-pressed conditions was compared in humid and saline atmospheres. These atmospheres were simulated in climatic test chambers that allow conditions similar to real working environments. The findings revealed improved corrosion behaviour of the cold-pressed coatings due to a reduced number of interconnected pores within the coatings and a negative influence of high volume fractions of SiC reinforcement.

* Corresponding author. Tel.: +34 91 3945227; fax: +34 91 3944357.
E-mail address: raularrabal@quim.ucm.es (R. Arrabal).

2. Experimental

2.1. Test materials

The chemical compositions of the Mg–Al–Zn alloys used in this work are listed in Table 1. Commercially pure or low purity Mg was used as the reference material. Mg and AZ31 wrought materials were supplied in plates of 3 mm thickness. The AZ80 and AZ91D casting alloys were supplied in the form of billets of 300 and 250 mm in diameter respectively. All the materials were supplied by Magnesium Elektron Ltd. (Manchester, United Kingdom).

2.2. Al/SiC thermal spray coatings

In order to enhance the adhesion of the coatings, the surfaces of the materials were sand-blasted with corundum of 1 mm mean diameter. Aluminium powder with a particle average size of 125 μm (Castolin: 99.5% Al rich) was mixed in a planetary ball mill at 225 rpm for 30 min with 5, 15 and 30 vol.% of SiC particles (SiCp) with an α-SiC 6H structure and an average particle size of 52 μm (interval 31.1–83.1 μm). SiCp were supplied by Navarro S.A. After mixing, the Al/SiCp composite coatings were applied on the surface of the magnesium substrates using a flame spray gun from Castolin (DS8000 model with a SSM40 modulus), which provided a thermal power of 28 kW by mixing oxygen at 4 bar and $2000 \, L \, h^{-1}$ with acetylene at 0.7 bar and $1800 \, L \, h^{-1}$. The main parameters used were: spraying distance of 20 cm, neutral flame (*i.e.* balanced amounts of oxygen and acetylene to get full combustion) and a transversal gun displacement over the sample surface of $150 \, cm \, min^{-1}$. The material feeding rate was $\sim 1.0 \, g \, s^{-1}$, and the average particle speed was $300 \, m \, s^{-1}$. A cold-pressing post-treatment was finally conducted at 32 MPa at room temperature for 3 min using a hydraulic press (model MC30, MECAMAQ S.L.). For all the experiments, duplicate specimens were prepared to guarantee the reliability of the results.

2.3. Specimen examination

Cross-sections of the coated specimens were wet ground through successive grades of SiC abrasive paper from P120 to P2000, followed by diamond finishing to 0.1 μm. Two etching reagents were used to reveal the constituents of the magnesium substrates: a) 5 s in Nital (5 mL nitric acid + 95 mL ethanol) for Mg, AZ80 and AZ91D materials and b) 5–10 s in Vilella reagent (0.6 g picric acid + 10 mL ethanol + 90 mL distilled water) for the AZ31 alloy. The constituents and were examined by scanning electron microscopy (SEM) using a JEOL JSM-6400 microscope equipped with Oxford Link energy dispersive X-ray (EDX) microanalysis hardware. Thicknesses of the coatings were measured at ten different locations by direct observation of the SEM cross-sections. Phase composition was investigated by low-angle X-ray diffraction (XRD) using a Philips X'Pert diffractometer ($K_\alpha Cu = 1.54056 \, Å$). Surface hardness was measured, applying a load of 5 kg for 20 s by using AKASHI AVK-AII Vickers hardness machine. Cited values are the average of ten measurements.

2.4. Gravimetric measurements

Gravimetric measurements were performed using specimens of $\sim 15 \, cm^2$ that were weighed before and after the tests using a Sartorius BP 211D scale with an accuracy of 0.00001 g. The edges of the coated specimens were protected by application of 45 "stopping-off" lacquer (MacDermid plc). Mass changes were calculated according to the expression $(M_f - M_i)/A$, where M_f is the final mass, M_i the initial mass and A the exposed surface area.

2.4.1. High humidity environment

The high relative humidity tests consisted of 24 h cycles performed in a saturated water vapour at 98% RH and 50 ± 1 °C during 28 days simulated by a humidity condensation cabinet CCK 300 (Dycometal). The temperature and the humidity were verified using a digital thermometer and hygrometer. At the end of the tests, the specimens were rinsed with deionized water, dried in warm air and weighed.

2.4.2. Salt fog environment

The specimens were hung in a CCl cabinet with a nylon thread and exposed to a 5 wt.% NaCl spray (pH 6.5–7.2) during 7 days. As recommended by ASTM B 117 standard, atomized air pressure of the saline solution was maintained in the range of 69 to $172 \, kN \, m^{-2}$ and the temperature inside the cabinet at 35 ± 1 °C. At the end of the tests, the specimens were washed with water below 38 °C to remove the saline deposits, dried in hot air and weighed.

2.5. Characterization of corrosion products

The tested specimens were examined by SEM in order to study the morphology and evolution of corrosion products formed on the material surface. Composition of the corrosion layer was examined by low-angle XRD.

3. Results and discussion

3.1. Microstructural characterization of the coatings

The microstructural characterization of the magnesium substrates was described elsewhere [22]. Fig. 1a–f shows the backscattered scanning electron (BSE) micrographs of the cross-sections of the as-sprayed (Al/SiCp-TS) and cold-pressed coatings (Al/SiCp-TS + CP). The substrate/coating interfaces presented some roughness due to the sand blasting pre-treatment. The Al/SiCp-TS coatings revealed an average thickness of 890 ± 50 μm with a very rough surface and interconnected pores or paths within the layer and at the substrate/coating interface (Fig. 1a–c, Fig. 2a, Fig. 3a). The high degree of porosity is typical of low velocity oxy-fuel processes like the one used in this study, where the relatively low particle velocities lead to reduced interparticle cohesive strength compared with other spraying technologies.

The cold-pressing post-treatment of the coatings under 32 MPa at room temperature for 3 min produced denser coatings (720 ± 10 μm) with smoother surfaces, absence of cracks and pores at the substrate/

Table 1
Chemical composition of investigated magnesium alloys.

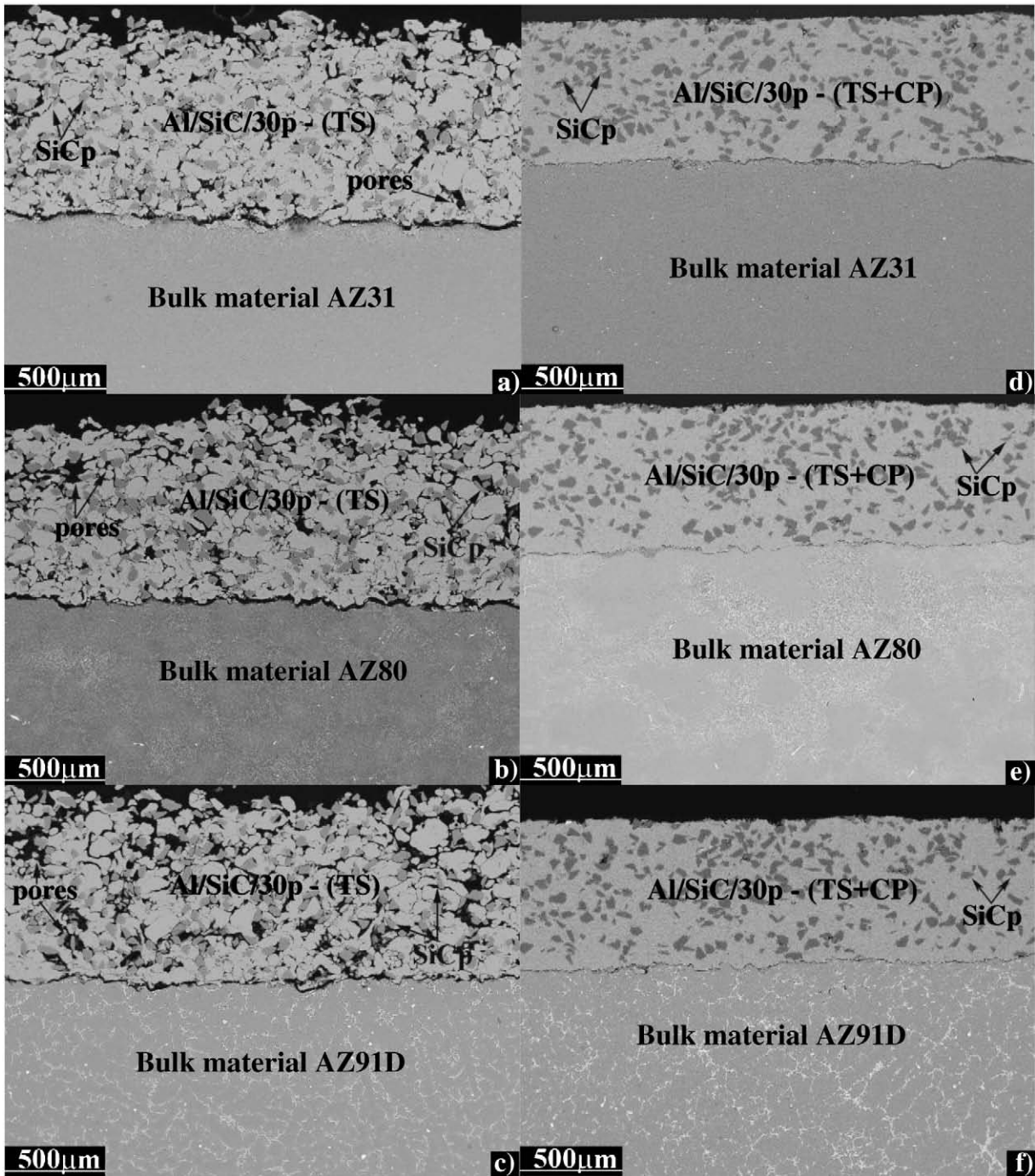| Material	Elements (wt.%)									
	Al	Zn	Mn	Si	Cu	Fe	Ni	Ca	Zr	Others
Mg (99.9%)	0.006	0.014	0.03	0.019	0.001	0.004	<0.001			
AZ31	3.1	0.73	0.25	0.02	<0.001	0.005	<0.001	<0.01	<0.001	<0.30
AZ80	8.2	0.46	0.13	0.01	<0.001	0.004				<0.30
AZ91D	8.8	0.68	0.30	0.01	<0.001	0.004	<0.008			<0.30

Fig. 1. BSE micrographs of the cross-sections of: (a–c) Al/SiCp-TS and (d–f) Al/SiCp-TS + CP coatings (AZ31, AZ80 and AZ91D alloys).

coating interface and more intimate bonding between the SiC particles and the aluminium matrix (Fig. 1d–f, Fig. 2b, Fig. 3b). These features suggested improved corrosion protection and adhesion of the coatings. At the used magnification, the SiC particles revealed a quite uniform distribution within the coatings (Fig. 1d–f) without formation of interfacial reaction products like the brittle Al_4C_3 (Fig. 3b). Inter-diffusion or compound layers between the aluminium coating and the substrate were not detected (Figs. 1 and 3).

Higher hardness values were observed after the cold-pressing post-treatment and with the increase in SiC volume fraction (Table 2). The Al/SiC/30p-TS + CP coatings exhibited hardness values that were higher than those of Mg and AZ31 materials and similar to those of untreated AZ80 and AZ91D magnesium alloys, whereas the Al/SiCp-TS coatings revealed the lowest surface hardness values associated with the high level of porosity of these layers. Therefore, from a mechanical point of view, the cold-pressed coatings are likely to provide better wear protection than the as-sprayed coatings.

3.2. Gravimetric results and corrosion morphology

3.2.1. High humidity environment

The gravimetric results of the test materials exposed to 98% RH at 50 °C are presented in Fig. 4. After 28 days, the highest mass gain was observed for Mg (0.5 mg cm^{-2}). This value decreased to 0.33 mg cm^{-2}, for the AZ31 alloy, and up to 0.2 mg cm^{-2} for the AZ80 and AZ91D alloys, demonstrating the positive influence of aluminium in the corrosion resistance of these magnesium alloys [23]. The increase in mass for the untreated materials was associated with the absorption of
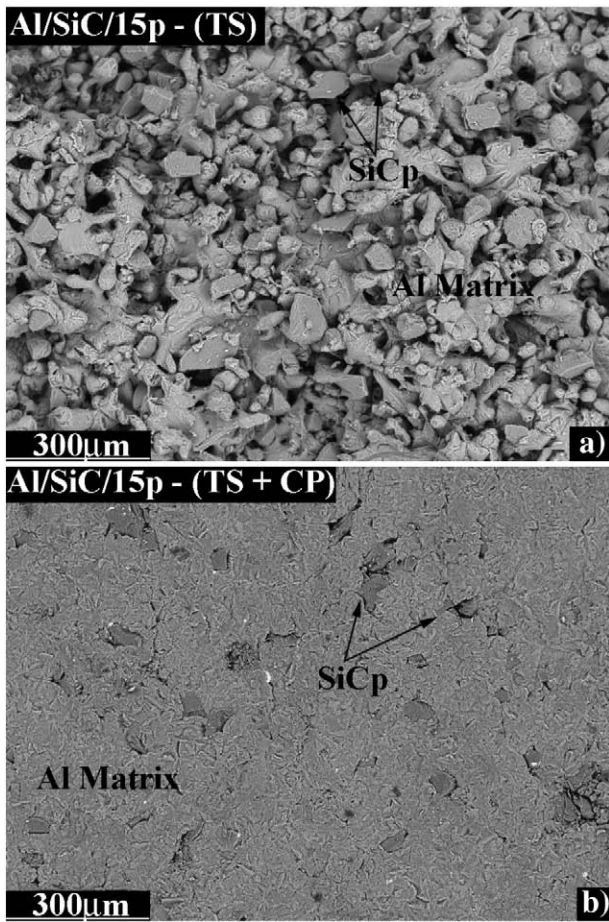
Fig. 2. Scanning electron micrographs of the plan views of (a) Al/SiC/15p-TS and (b) Al/SiC/15p-TS + CP coatings.
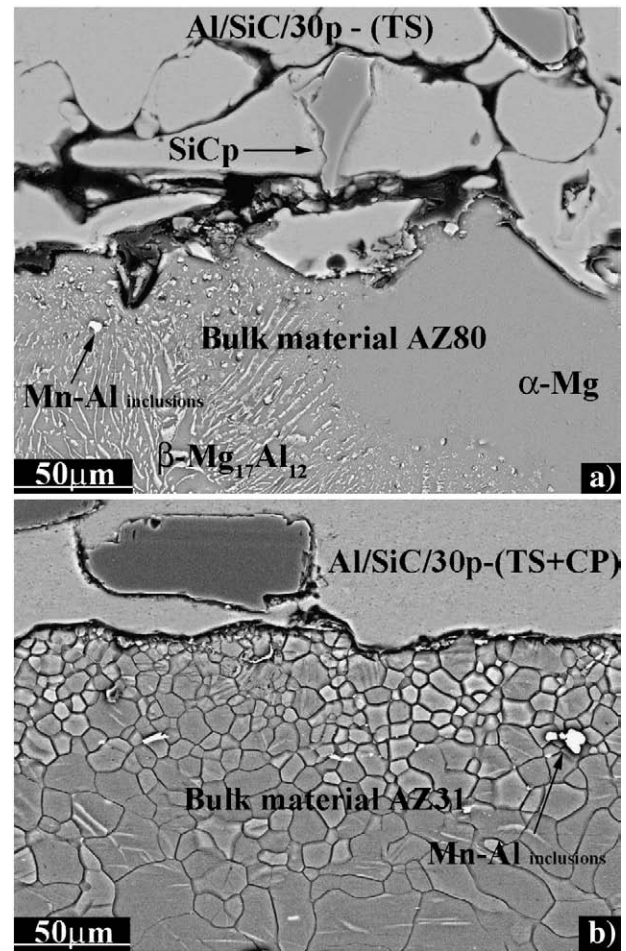

Fig. 3. Scanning electron micrographs of the substrate/coating interfaces of (a) Al/SiC/30p-TS and (b) Al/SiC/30p-TS + CP.

H_2O and CO_2 and the formation of corrosion products on the surface [22].

The specimens with the as-sprayed Al/SiCp coatings revealed initial mass losses in the interval between 0.05 mg cm^{-2} and 0.27 mg cm^{-2} after 2–4 days. This may be related to either corrosion of the coating or the magnesium substrate. With increasing exposure times, the mass gain increased once again due to accumulation of corrosion products. In the case of the Al/SiCp-TS + CP coatings, the rate of formation of corrosion products decreased with time, suggesting the formation of corrosion products slightly more protective compared with those formed in the untreated and Al/SiCp-TS specimens. In general, the final mass gain values were higher for the coatings with a higher volume fraction of SiC reinforcement, regardless of the application of the cold-pressing post-treatment (Fig. 4).

The surface appearance of the Al/SiCp coatings exposed to 98% RH at 50 °C revealed negligible surface degradation of both as-sprayed and cold-pressed coatings after 28 days (Fig. 5). However, a more detailed examination by SEM revealed signs of galvanic corrosion at the substrate/coating interfaces for the specimens with the Al/SiCp-TS coatings (Fig. 6a). EDX analysis of the corrosion products located at this interface gave an average composition of 65.3% O and 34.7% Mg (at.%), which suggested $Mg(OH)_2$ as the main corrosion product. This confirmed the presence of through-pores or micro-channels in the as-sprayed coatings that facilitated the penetration of the aggressive medium towards the magnesium substrates. The incorporation of a higher number of SiC particles rendered coatings with lower anti-corrosion properties and therefore, increased accumulation of corrosion products at the substrate/coating interface. This can be attributed to a higher degree of porosity with increasing the volume fraction of reinforcement, since SiC particles have poor wettability with the aluminium splats [21].

The specimens with the cold-pressed Al/SiCp coatings did not reveal galvanic corrosion phenomena between the coating and magnesium substrates after 28 days of exposure to the high humidity environment (Fig. 6b). Instead, only minor corrosion attack was observed at the aluminium/SiCp interfaces in the outermost surface of the coatings (Fig. 7). These interfaces are known to be preferential sites for corrosion attack in Al/SiC composites due to several factors such as accumulation of defects, porosity and discontinuity of the passive layer [24]. The cross-sectional examination of the corroded areas in the Al/SiCp-TS + CP coatings confirmed the shallow corrosion penetration around the SiC particles with formation of aluminium corrosion products (Fig. 8).

Table 2
Surface hardness values of pure Mg, AZ31, AZ80 and AZ91D materials with Al/SiCp coatings.

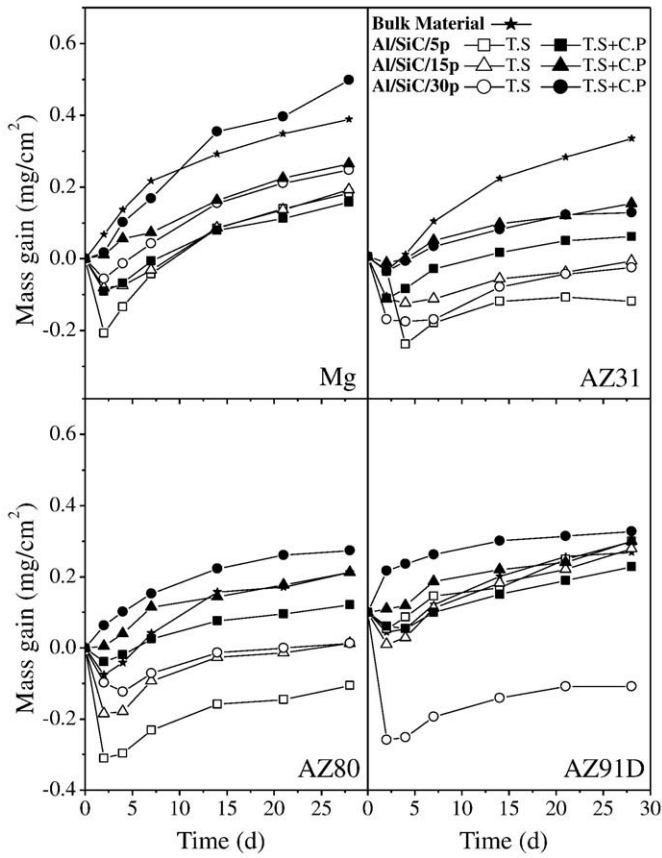| Material	%vol. SiCp	Mg	AZ31	AZ80	AZ91D
Untreated	–	42.2	65.6	99.2	79.8
Al/SiCp-TS	5	16.6	16.3	15.8	16.7
	15	17.3	16.9	17.5	17.4
	30	20.3	19.8	20.2	19.6
Al/SiCp-TS + CP	5	53.0	54.8	55.7	53.3
	15	57.8	58.2	56.4	59.6
	30	87.2	83.8	85.1	83.1

Fig. 4. Mass gain vs. immersion time for the materials exposed to high humidity environment (98% RH at 50 °C).

Table 3 shows the kinetic laws calculated from the gravimetric measurements in high humidity atmosphere using a linear or parabolic expression ($y = b \cdot t$, $y^2 = b \cdot t$). The increase in aluminium content in the bulk composition of the untreated magnesium alloys caused a decrease in the kinetic constant by up to 2 times. For exposure times above 7 days, the kinetic constants of the specimens with as-sprayed and cold-pressed coatings were similar and approximately 3 times smaller than those of untreated materials. Therefore, in high humidity atmosphere the galvanic couple observed between
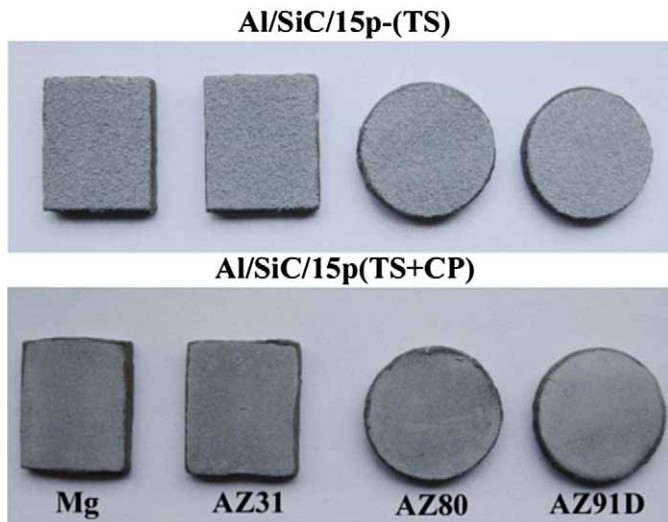

Fig. 5. Surface appearance of Al/SiC/15p-TS and Al/SiC/15p-TS + CP coatings after exposure to high humidity environment for 28 days.
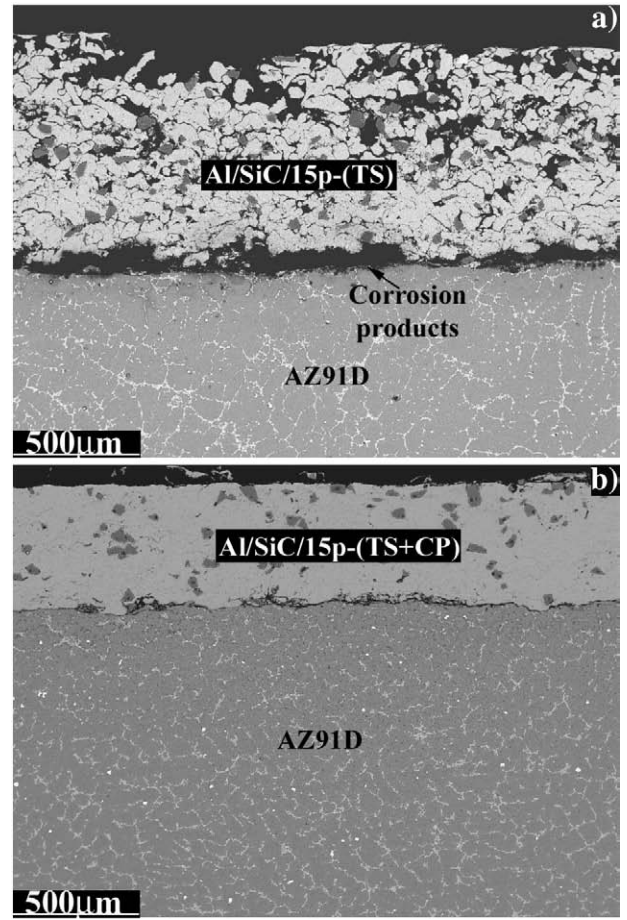

Fig. 6. BSE micrographs of the cross-sections of the AZ91D alloy with the (a) Al/SiC/15p- TS and (b) Al/SiC/15p-TS + CP coatings after 28 days of exposure to high humidity environment.

the as-sprayed coatings and the magnesium substrates did not significantly increase the corrosion rate compared with the denser cold-pressed coatings.

3.2.2. Salt fog environment

Fig. 9 and Table 4 show the gravimetric results of test materials exposed to salt fog environment for 7 days. For the untreated materials, Mg revealed rapid mass loss and was disintegrated after 2 days. A considerable enhancement of the corrosion resistance was
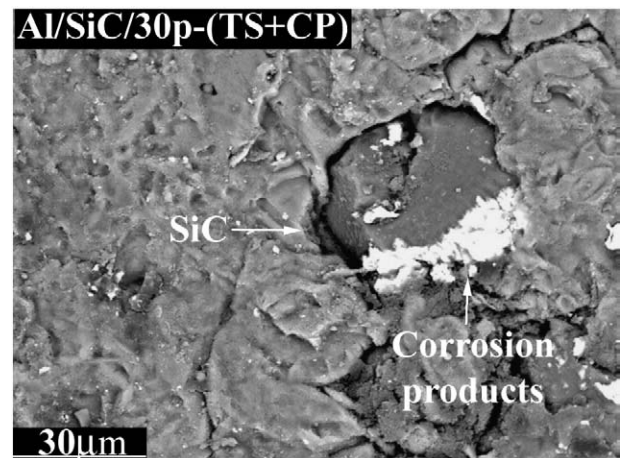

Fig. 7. BSE micrograph of the Al/SiC/30p-TS + CP coating after exposure for 28 days to high humidity environment.
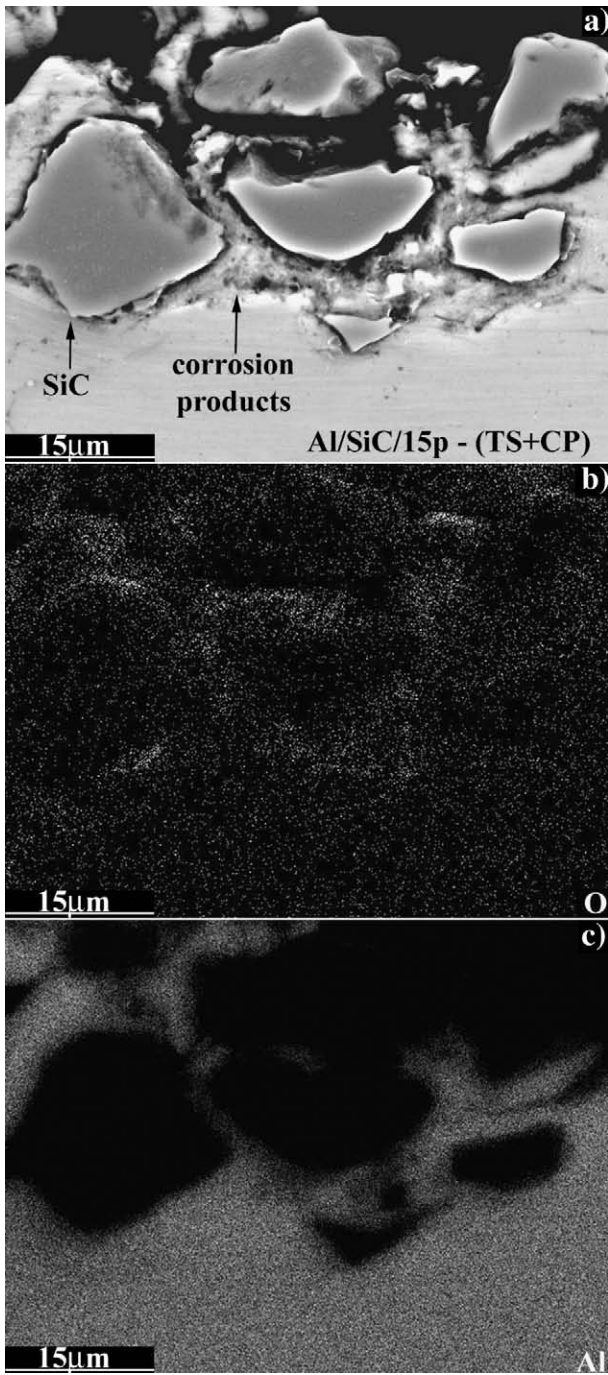
Fig. 8. (a) BSE micrograph and X-ray elemental maps of (b) O and (c) Al of the cross-section of the Al/SiC/15p-TS + CP coating after exposure to high humidity environment for 28 days.

Table 3
Kinetic laws of materials exposed to high humidity environment.

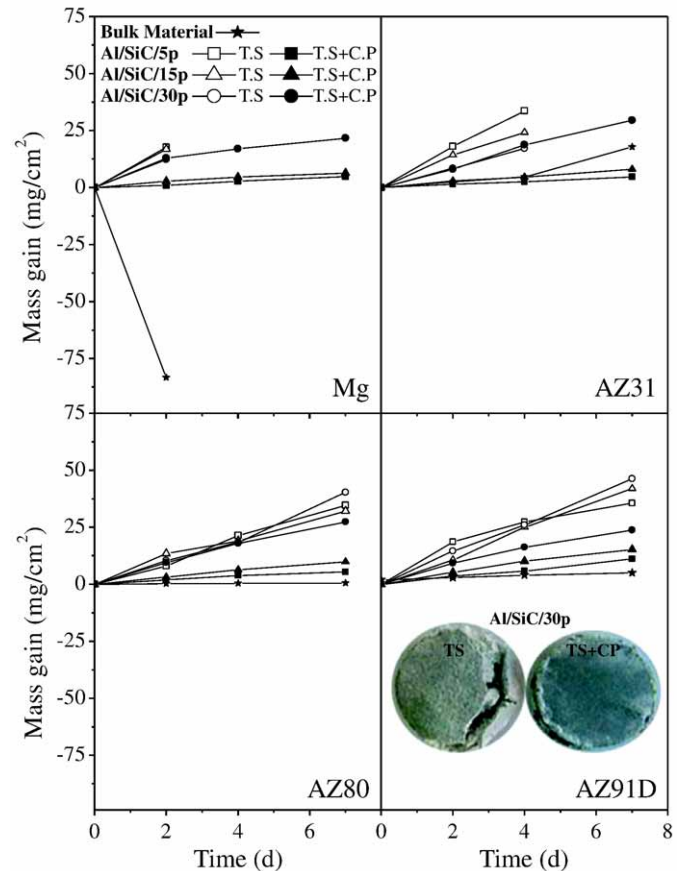| Material		%vol. SiCp	Kinetic law: $y=b\cdot t; y^2=b\cdot t$; [y (mg/cm²), t (d)]	Time (d)	r^2
Mg	Untreated	–	$y=1.6\times10^{-2}t$	$7\leq t\leq28$	0.99
	Al/SiCp-TS	5	$y^2=1.5\times10^{-2}t$	$4\leq t\leq28$	0.97
		15	$y^2=0.9\times10^{-2}t$	$4\leq t\leq28$	0.96
		30	$y^2=0.7\times10^{-2}t$	$4\leq t\leq28$	0.97
	Al/SiCp-TS + CP	5	$y^2=0.4\times10^{-2}t$	$2\leq t\leq28$	0.96
		15	$y^2=0.4\times10^{-2}t$	$2\leq t\leq28$	0.96
		30	$y^2=0.6\times10^{-2}t$	$0\leq t\leq28$	0.97
AZ31	Untreated	-	$y=1.1\times10^{-2}t$	$7\leq t\leq28$	0.92
	Al/SiCp-TS	5	$y^2=0.1\times10^{-2}t$	$7\leq t\leq28$	0.80
		15	$y^2=0.1\times10^{-2}t$	$7\leq t\leq28$	0.98
		30	$y^2=0.3\times10^{-2}t$	$7\leq t\leq28$	0.94
	Al/SiCp-TS + CP	5	$y^2=0.2\times10^{-2}t$	$4\leq t\leq28$	0.96
		15	$y^2=0.2\times10^{-2}t$	$4\leq t\leq28$	0.97
		30	$y^2=0.2\times10^{-2}t$	$4\leq t\leq28$	0.97
AZ80	Untreated	–	$y=0.8\times10^{-2}t$	$7\leq t\leq28$	0.92
	Al/SiCp-TS	5	$y^2=0.3\times10^{-2}t$	$4\leq t\leq28$	0.95
		15	$y^2=0.3\times10^{-2}t$	$4\leq t\leq28$	0.89
		30	$y^2=0.1\times10^{-2}t$	$7\leq t\leq28$	0.91
	Al/SiCp-TS + CP	5	$y^2=0.2\times10^{-2}t$	$4\leq t\leq28$	0.96
		15	$y^2=0.3\times10^{-2}t$	$0\leq t\leq28$	0.96
		30	$y^2=0.3\times10^{-2}t$	$0\leq t\leq28$	0.97
AZ91D	Untreated	–	$y=0.8\times10^{-2}t$	$7\leq t\leq28$	0.92
	Al/SiCp-TS	5	$y^2=0.4\times10^{-2}t$	$4\leq t\leq28$	0.96
		15	$y^2=0.4\times10^{-2}t$	$4\leq t\leq28$	0.96
		30	$y^2=0.2\times10^{-2}t$	$4\leq t\leq28$	0.92
	Al/SiCp-TS + CP	5	$y^2=0.2\times10^{-2}t$	$7\leq t\leq28$	0.99
		15	$y^2=0.2\times10^{-2}t$	$0\leq t\leq28$	0.96
		30	$y^2=0.6\times10^{-2}t$	$0\leq t\leq28$	0.97

Fig. 9. Mass gain vs. immersion time for the materials exposed to salt fog environment and surface appearance of as-sprayed and cold-pressed coatings after 7 days of test.

observed for the magnesium alloys containing aluminium. Thus, after 7 days, the AZ31, AZ80 and AZ91D alloys presented mass gain values of 18 mg cm⁻², 0.6 mg cm⁻² and 7 mg cm⁻² respectively. The Al/SiCp-TS specimens revealed poor corrosion performance in salt fog environment. The mass gain values were in the interval between 13 and 18 mg cm⁻² after 2 days, and coating spalling was evident for exposure times below 7 days. The Al/SiCp-TS + CP specimens revealed lower mass gain (~ 5–30 mg cm⁻²) than the as-sprayed specimens at the end of the test, however, coating spalling was observed for times above 7 days (Fig. 9). The addition of reinforcement revealed a detrimental effect on the corrosion behaviour of the cold-pressed coatings, especially for 30 vol.% SiCp. Thus, the calculated kinetic

Table 4
Kinetic laws of materials exposed to salt fog environment.

Material		%vol. SiCp	Kinetic law: $y = b \cdot t$; [y (mg/cm^2), t (d)]	Time (d)	r^2
Mg	Untreated	–	$y = -41.6t$	$0 \leq t \leq 2$	1
	Al/SiCp-TS	5	$y = 8.8t$	$0 \leq t \leq 2$	1
		15	$y = 8.4t$	$0 \leq t \leq 2$	1
		30	$y = 6.2t$	$0 \leq t \leq 2$	1
	Al/SiCp-TS + CP	5	$y = 0.7t$	$0 \leq t \leq 7$	0.99
		15	$y = 0.9t$	$0 \leq t \leq 7$	0.92
		30	$y = 2.9t$	$0 \leq t \leq 7$	0.94
AZ31	Untreated	–	$y = 2.5t$	$0 \leq t \leq 7$	0.95
	Al/SiCp-TS	5	$y = 8.4t$	$0 \leq t \leq 7$	0.99
		15	$y = 6.0t$	$0 \leq t \leq 7$	0.99
		30	$y = 4.3t$	$0 \leq t \leq 7$	1
	Al/SiCp-TS + CP	5	$y = 0.6t$	$0 \leq t \leq 7$	0.99
		15	$y = 1.1t$	$0 \leq t \leq 7$	0.99
		30	$y = 4.3t$	$0 \leq t \leq 7$	0.99
AZ80	Untreated	–	$y = 0.1t$	$0 \leq t \leq 7$	0.97
	Al/SiCp-TS	5	$y = 5.1t$	$0 \leq t \leq 7$	0.99
		15	$y = 4.4t$	$0 \leq t \leq 7$	0.98
		30	$y = 5.7t$	$0 \leq t \leq 7$	0.97
	Al/SiCp-tS + CP	5	$y = 0.8t$	$0 \leq t \leq 7$	0.98
		15	$y = 1.4t$	$0 \leq t \leq 7$	0.99
		30	$y = 3.9t$	$0 \leq t \leq 7$	0.99
AZ91D	Untreated	–	$y = 0.4t$	$0 \leq t \leq 7$	0.99
	Al/SiCp-TS	5	$y = 4.9t$	$0 \leq t \leq 7$	0.95
		15	$y = 6.1t$	$0 \leq t \leq 7$	0.99
		30	$y = 6.5t$	$0 \leq t \leq 7$	0.99
	Al/SiCp-TS + CP	5	$y = 1.6t$	$0 \leq t \leq 7$	0.99
		15	$y = 2.2t$	$0 \leq t \leq 7$	0.99
		30	$y = 3.4t$	$0 \leq t \leq 7$	0.98

constants increased by ~ 2–7 times when the volume fraction of SiC particles increased from 5 to 30% (Table 4). This negative effect was attributed to a higher number of pores in the coatings with increasing volume fraction of reinforcement, which can be explained by the poor wettability between the aluminium splats and the SiC particles and the negligible plastic deformation of these ceramic particles during the cold-pressing post-treatment.

3.3. XRD results

Fig. 10 discloses the low-angle XRD study (incident angle 1°) of the investigated materials after exposure to humid environment for 28 days. For the untreated materials, the main corrosion products were magnesium hydroxide (brucite ($Mg(OH)_2$) and hydrated magnesium carbonate hydroxide (hydromagnesite $Mg_5(CO_3)_4(OH)_2 \cdot 4H_2O$)) [23]. The identified peaks for the Al/SiCp-TS specimens corresponded to the coating constituents (Al and SiC) and bayerite (β-$Al_2O_3.3H_2O$), which indicated some corrosion of the Al/SiCp coatings before galvanic corrosion of the magnesium substrates. The corrosion products observed by SEM at the coating/substrate interface (Fig. 6) were not detected by the low-angle X-ray study due to the inherent limitations of this technique, however, they were probably constituted of $Mg(OH)_2$ and magnesium carbonates due to reaction of atmospheric CO_2 with $Mg(OH)_2$ [25]. For the Al/SiCp-TS + CP specimens, the XRD patterns revealed the components of the coatings and higher intensity peaks of bayerite. This higher intensity of aluminium corrosion products compared with the Al/SiCp-TS specimens was attributed to the preferential formation of bayerite in the outermost regions of the coatings (Fig. 8) rather than within the pores or micro-channels in the highly porous as-sprayed coatings. The main corrosion products responsible for the detachment of the coatings in salt fog environment were identified as $Mg(OH)_2$ (Fig. 11).

4. Conclusions

1. The as-sprayed Al/SiCp coatings revealed a high level of porosity with poor contact between the deposited splats of aluminium and SiC particles. The cold-pressing post-treatment reduced the number of interconnected pores and produced more homogeneous and smoother coatings with improved bonding at the substrate/coating interface. The formation of diffusion layers or degradation of SiC particles was not observed.

2. In high humidity environment, the specimens with the as-sprayed Al/SiCp coatings revealed minor surface degradation with formation of bayerite in the outer regions of the coatings and partial dissolution of the magnesium substrates due to galvanic corrosion. This was motivated by the through-coating pores and the different nobility of aluminium and magnesium. The Al/SiCp coatings were more efficient against corrosion after the cold-pressing post-treatment due to the reduced number of interconnected pores. Thus, corrosion products consisting of β-$Al_2O_3 \cdot 3H_2O$ were only localised at the Al/SiCp interfaces in the surface of the coatings.

3. In salt fog environment, the as-sprayed and cold-pressed coatings revealed much higher corrosion rates than in the humid test and the accumulation of corrosion products, as a consequence of galvanic corrosion at the coating/substrate interface, facilitated coating spalling after several days of exposure.

4. The ceramic reinforcement revealed a negative effect on the corrosion behaviour of magnesium substrates coated with the as-sprayed and cold-pressed Al/SiCp coatings. This effect was more
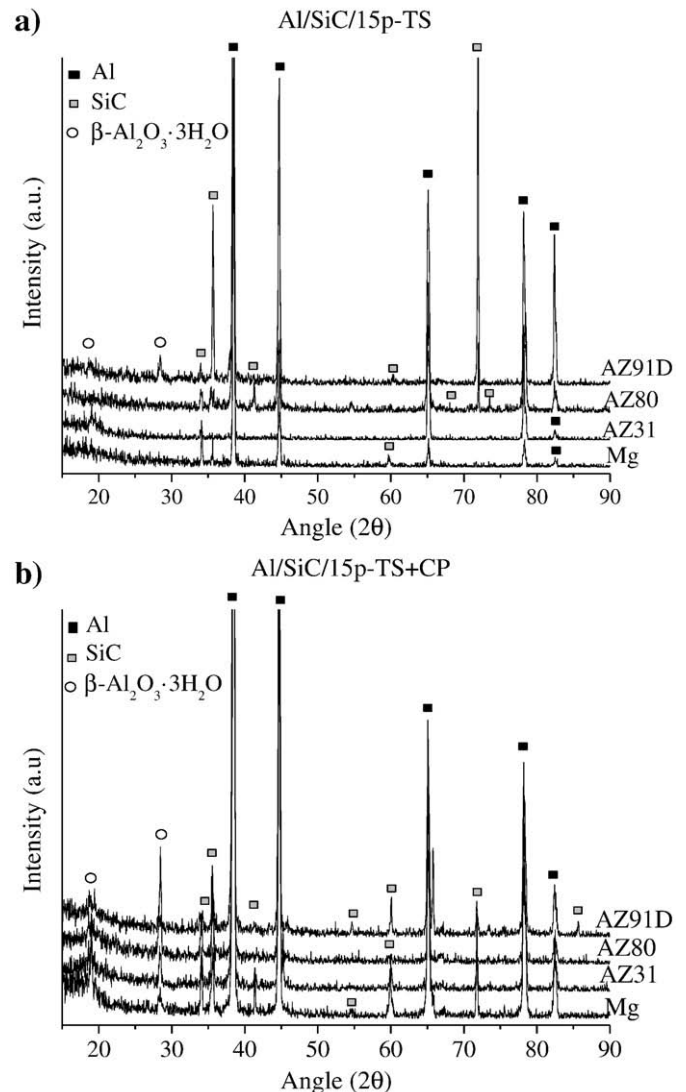

Fig. 10. Low-angle XRD (incident angle 1°) study of (a) Al/SiC/15p-TS and (b) Al/SiCp/15p-TS + CP specimens after exposure to high humidity environment for 28 days.
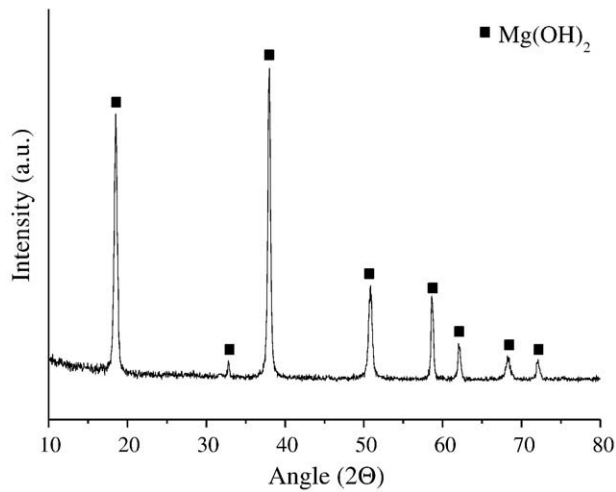
Fig. 11. XRD study of the corrosion products formed at the substrate/coating interface of the AZ80 alloy with the Al/SiCp/30p-TS coating after exposure to salt fog for 7 days.

noticeable in the salt fog test and for high volume fractions of reinforcement. This negative effect was associated with a higher level of porosity with increasing volume fractions of SiC particles due to their poor wettability with aluminium and insignificant plastic deformation during the applied post-treatment.

Acknowledgements

References

[1] H. Friedrich, S. Schumann, J. Mater. Process. Technol. 117 (2001) 276.
[2] L. Whitby, in: F.L. LaQue, H.R. Copson (Eds.), Corrosion resistance of metals and alloys, Reinhold, New York, 1963, p. 169.
[3] J.F. King, A.G. Gordon, P. Lyon, in: E.W. Lee, N.J. Kim (Eds.), Proc. Symp. Light Weight Alloys for Aerospace Applications, 1991, p. 423.
[4] P. Kurze, in: H. Friedrich, B.L. Mordike (Eds.), Magnesium Technology, Metallurgy, Desing Data, Applications, Springer-Verlag Berlin, Germany, 2006, p. 431.
[5] J.E. Gray, B. Luan, J. Alloys Compd. 336 (2002) 88.
[6] B. Gerard, Surf. Coat. Technol. 201 (2006) 2028.
[7] M. Parco, L. Zhao, J. Zwick, K. Bobzin, E. Lugscheider, Surf. Coat. Technol. 201 (2006) 3269.
[8] Y. Tao, T. Xiong, C. Sun, H. Jin, H. Du, T. Li, Appl. Surf. Sci. 256 (2009) 261.
[9] A. Pardo, P. Casajús, M. Mohedano, A.E. Coy, F. Viejo, B. Torres, E. Matykina, Appl. Surf. Sci. 255 (2009) 6968.
[10] W. Zhongshan, L. Liufa, D. Wenjiang, Mater. Sci. Forum 488–489 (2005) 685.
[11] L. Chiu, H. Lin, C. Chen, C. Yang, C. Chang, J. Wu, Mater. Sci. Forum 419–422 (2003) 909.
[12] L. Chiu, C. Chen, C. Yang, Surf. Coat. Technol. 191 (2005) 181.
[13] B. Wielage, T. Grund, H. Pokhmurska, C. Rupprecht, T. Lampke, Key Eng. Mater. 384 (2008) 99.
[14] H. Pokhmurska, B. Wielage, T. Lampke, T. Grund, M. Student, N. Chervinska, Surf. Coat. Technol. 202 (2008) 4515.
[15] A. Pardo, M.C. Merino, M. Mohedano, P. Casajús, A.E. Coy, R. Arrabal, Surf. Coat. Technol. 203 (2009) 1252.
[16] R. Arrabal, A. Pardo, M.C. Merino, S. Merino, P. Casajús, M. Mohedano, P. Rodrigo, Corrosion 65 (2009) 817.
[17] A. Pardo, M.C. Merino, P. Casajus, M. Mohedano, R. Arrabal, E. Matykina, Mater. Corros. 60 (2009) 939.
[18] P. Rodrigo, M. Campo, B. Torres, M.D. Escalera, E. Otero, J. Rams, Appl. Surf. Sci. 255 (2009) 9174.
[19] J.D. Majumdar, B.R. Chandra, R. Galun, B.L. Mordike, I. Manna, Compos. Sci. Technol. 63 (2003) 771.
[20] M. Campo, M. Carboneras, M.D. Lopez, B. Torres, P. Rodrigo, E. Otero, J. Rams, Surf. Coat. Technol. 203 (2009) 3224.
[21] M. Campo, M.D. Escalera, B. Torres, J. Rams, A. Ureña, Rev. Metal. 43 (2007) 359.
[22] S. Feliu Jr., A. Pardo, M.C. Merino, A.E. Coy, F. Viejo, R. Arrabal, Appl. Surf. Sci. 255 (2009) 4102.
[23] R. Arrabal, A. Pardo, M.C. Merino, S. Merino, M. Mohedano, P. Casajús, Mater. Corros. (2009) In press.
[24] M. Metzger, S.G. Fishman, Ind. Eng. Chem. Prod. Res. 22 (1983) 296.
[25] M. Jönsson, D. Persson, C. Leygraf, Corros. Sci. 50 (2008) 1406.